The Astrophysical Journal, 652:948–954, 2006 December 1
© 2006. The American Astronomical Society. All rights reserved. Printed in U.S.A.

ANALYSIS AND INTERPRETATION OF HARD X-RAY EMISSION FROM THE BULLET CLUSTER (1ES 0657−558), THE MOST DISTANT CLUSTER OF GALAXIES OBSERVED BY *RXTE*

Vahé Petrosian,[1,2,3] Greg Madejski,[2,4] and Kevin Luli[1]

Received 2006 June 19; accepted 2006 August 11

ABSTRACT

Evidence for nonthermal activity in clusters of galaxies is well established from radio observations of synchrotron emission by relativistic electrons. New windows in the extreme-ultraviolet and hard X-ray ranges have provided more powerful tools for the investigation of this phenomenon. Detections of hard X-rays in the 20–100 keV range have been reported for several clusters of galaxies, notably from Coma and others. Based on these earlier observations we identified the relatively high-redshift cluster 1ES 0657−558 (also known as RX J0658−5557) as a good candidate for hard X-ray observations. This cluster, also known as the Bullet Cluster, has many other interesting and unusual features, most notably that it is undergoing a merger, clearly visible in the X-ray images. Here we present results from successful *RXTE* observations of this cluster. We summarize past observations and their theoretical interpretation that guided us in the selection process. We describe the new observations and present the constraints we can set on the flux and spectrum of the hard X-rays. Finally, we discuss the constraints one can set on the characteristics of accelerated electrons that produce the hard X-rays and the radio radiation.

Subject headings: acceleration of particles — galaxies: clusters: individual (1ES 0657−558, RX J0658−5557) — X-rays: galaxies: clusters

Online material: color figures

1. INTRODUCTION

The intracluster media (ICM) of several clusters of galaxies show, in addition to the well-studied thermal bremsstrahlung (TB) emission dominating in the ~2–10 keV soft X-ray (SXR) region, growing evidence for nonthermal activity. This activity was first observed in a form of diffuse radio radiation (classified either as relic or halo sources). The first cluster with diffuse emission detected in the radio band was Coma, and recent systematic searches have identified more than 40 clusters with halo or relic sources. In the case of Coma, the radio spectrum can be represented by a broken power law (Rephaeli 1979) or by a power law with a rapid steepening (Thierbach et al. 2003) or with an exponential cutoff (Schlickeiser et al. 1987). There is little doubt that this radiation is due to synchrotron emission by a population of relativistic electrons with similar spectra; however, from radio observations alone one cannot determine the energy of the electrons or the strength of the magnetic field. Additional observations or assumptions are required. Minimum total (particles plus field) energy or equipartition assumptions imply a magnetic field strength of $B \sim 1\ \mu$G, in rough agreement with the Faraday rotation measurements (e.g., Kim et al. 1990), and a population of relativistic electrons with Lorentz factor $\gamma \sim 10^4$. In the papers cited above, it was also realized that because the energy density of the cosmic microwave background (CMB) radiation (temperature T_0) $u_{\rm CMB} = 4 \times 10^{-13}(T_0/2.8\ {\rm K})^4$ ergs cm^{-3} is larger than the magnetic energy density $u_{\rm B} = 3 \times 10^{-14}(B/\mu{\rm G})^2$ ergs cm^{-3}, most of the energy of the relativistic electrons would be radiated via inverse Compton (IC) scattering of the CMB photons, producing a broad photon spectrum (similar to that observed in the radio band) around 50 keV (for $\gamma \sim 10^4$). Thus, one expects a higher flux of nonthermal X-ray radiation than of radio radiation. Detection of hard X-rays would then break the degeneracy and allow determination of the magnetic field and the energy of the radiating electrons. Moreover, since the redshift dependence of the CMB photons is known, then in principle, the cosmological evolution of these quantities can also be investigated.

While the detectability of such radiation would be easiest in the soft X-ray range, for which very sensitive imaging instruments are available, in reality this range is masked by the prominent thermal bremsstrahlung emission, a general characteristic of clusters. With this in mind, the most promising is either the hard X-ray (HXR) band, beyond the energies at which TB flux dominates, or alternatively, in the very soft X-ray or extreme-ultraviolet (EUV) regime. Recently, HXR emission (in the 20–80 keV range) at significant levels above that expected from the thermal gas was detected by instruments on board the *BeppoSAX* and *Rossi X-Ray Timing Explorer* (*RXTE*) satellites from Coma (Rephaeli et al. 1999; Fusco-Femiano et al. 1999, 2004;[5] Rephaeli & Gruber 2002), Abell 2319 (Gruber & Rephaeli 2002), and Abell 2256 (Fusco-Femiano et al. 2000, 2005; Rephaeli & Gruber 2003), as well as a marginal (~3 σ) detection from Abell 754 and an upper limit on Abell 119 (Fusco-Femiano et al. 2003). We also note that a possible recent detection of nonthermal X-rays, albeit at lower energies, has been reported from a poor cluster, IC 1262, by Hudson et al. (2003). All those clusters are in the redshift range $0.023 < z < 0.056$. A notable recent exception at a higher redshift is Abell 2163 (Rephaeli et al. 2006), for which the reported nonthermal flux is consistent with the upper limit set by *BeppoSAX* (Feretti et al. 2001). It should also be noted that excess radiation was detected in the 0.1–0.4 keV band by *Röntgensatellit* (*ROSAT*), *BeppoSAX*, and *XMM-Newton* and that in the EUV

[1] Department of Physics, Stanford University, Stanford, CA 94305; vahe@astronomy.stanford.edu.
[2] Kavli Institute for Particle Astrophysics and Cosmology, Stanford University, Stanford, CA 94305.
[3] Department of Applied Physics, Stanford University, Stanford, CA 94305.
[4] Stanford Linear Accelerator Center, 2575 Sand Hill Road, Menlo Park, CA 94025.

[5] The results of this paper have been challenged by an analysis performed with different software by Rossetti & Molendi (2004).

region (0.07–0.14 keV) similar excess radiation was detected by the *Extreme Ultraviolet Explorer* from Coma (Lieu et al. 1996) and some other clusters. A cooler ($kT \sim 2$ keV) component and IC scattering of CMB photons by lower energy ($\gamma \sim 10^3$) electrons are two possible ways of producing this excess radiation. However, some of the observations and the emission process are still controversial (see Bowyer 2003).

Here we present results from ∼309 ks *RXTE* observations of cluster 1ES 0657−558 (also known as RX J0658−5557) with a considerably higher redshift of $z = 0.296$, which manifests many other interesting features (Markevitch 2005). All those hard X-ray observations encompass a wide range of temperature, redshift, and luminosity, especially with the addition of 1ES 0657−558, indicating that HXR emission may be a common property of all clusters with significant diffuse radio emission. In the next section we give brief descriptions of the emission processes and the considerations that led to the selection of 1ES 0657−558 as a target for HXR observations by *RXTE*. In § 3 we describe the observations and the results from our spectral fits. Finally, in § 4 we discuss the significance of our results and their implication for the radiation and acceleration mechanisms.

2. EMISSION PROCESSES AND TARGET SELECTION

As stated above, electrons of similar energies can be responsible for both the IC-HXR and synchrotron-radio emission, and the ratio of these fluxes depends primarily on the ratio of the photon (CMB in our case) to magnetic field energy densities. For a population of relativistic electrons with the spectrum $N(\gamma) = K\gamma^{-p} = N_{\rm total}(p-1)\gamma^{-p}\gamma_{\rm min}^{p-1}$ for $\gamma > \gamma_{\rm min}$, the spectrum of the emitted luminosities of both radiation components is given by

$$\nu L_i(\nu) = cr_0^2 N_{\rm total}\gamma_{\rm min}^{p-1} u_i A_i(p)\left(\nu/\nu_{{\rm cr},i}\right)^{2-\Gamma}, \qquad (1)$$

where r_0 is the classical electron radius, c is the speed of light, and $\Gamma = (p+1)/2$ is the photon number spectral index.[6]

For synchrotron $\nu_{\rm cr,synch} = 3\gamma_{\rm min}^2\nu_{B_\perp}/2$, with $\nu_{B_\perp} = eB_\perp/(2\pi mc)$ and $u_{\rm synch} = B^2/(8\pi)$, and for IC u_i is the soft photon energy density and $\nu_{\rm cr,IC} = \gamma_{\rm min}^2\langle h\nu\rangle$. For blackbody photons $u_{\rm IC} = (8\pi^5/15)(kT)^4/(hc)^3$ and $\langle h\nu\rangle = 2.8kT$. The A_i are some simple functions of the electron index p and are of the order of unity (see, e.g., Rybicki & Lightman 1979). Because we know the temperature of the CMB photons, from the observed ratio of fluxes we can determine the strength of the magnetic field. For Coma, this requires the volume-averaged magnetic field to be $\bar{B} \sim 0.1$ μG, while equipartition gives $\bar{B} \sim 0.4$ μG and Faraday rotation measurements give an average line-of-sight field of $\bar{B}_{\rm l} \sim 3$ μG (Giovannini et al. 1993; Kim et al. 1990; Clarke et al. 2001; Clarke 2003). (In general the Faraday rotation measurements of most clusters give $B > 1$ μG [see, e.g., Govoni et al. 2003].) However, there are several factors that may resolve this discrepancy. First, the last value assumes a chaotic magnetic field with a scale of a few kiloparsecs, which is not a directly measured quantity (see, e.g., Carilli & Taylor 2002). Second, the accuracy of these results has been questioned by Rudnick & Blundell (2003) and defended by Govoni & Feretti (2004) and others. Third, as pointed out by Brunetti et al. (2001), a strong gradient in the magnetic field can reconcile the difference between the volume- and line-of-sight–averaged measurements. Finally, as pointed out by Petrosian (2001, hereafter P01), this discrepancy can be alleviated by a more realistic electron spectral distribution (e.g., the spectrum with exponential cutoff suggested by Schlickeiser et al. 1987) and/or a nonisotropic pitch angle distribution. In addition, for a population of clusters observational selection effects come into play and may favor Faraday rotation detection in high-B clusters, which would have a weaker IC flux relative to synchrotron.

A second possibility is that the HXR radiation is produced via bremsstrahlung by a population of electrons with energies comparable to and larger than the HXR photons. If a thermal distribution of electrons is the source of this radiation, such electrons must have a much higher temperature than the gas responsible for the SXR emission. For production of HXR flux up to 50 keV this requires a gas with $kT > 30$ keV and (for Coma) with an emission measure about 10% of that of the SXR-producing plasma. Heating the plasma to such high temperatures and maintaining it in view of rapid equilibration expected by classical Spitzer conduction is problematic. It has also been suggested by various authors (see, e.g., Enßlin et al. 1999; Blasi 2000) that the HXR radiation is due to nonthermal bremsstrahlung (NTB) by a power-law distribution of electrons in the 10–100 keV range. However, it was shown in P01 that the NTB process faces a serious difficulty that is hard to circumvent: compared to Coulomb losses the bremsstrahlung yield is very small, $Y_{\rm brem} \sim 3\times10^{-6}(E/25\ {\rm keV})^{3/2}$ (see Petrosian 1973). Thus, to maintain production of a HXR luminosity of 4×10^{43} ergs s^{-1} (observed for Coma), a power of $L_{\rm HXR}/Y_{\rm brem} \sim 10^{49}$ ergs s^{-1} must be continuously fed into the ICM, increasing its temperature to $T \sim 10^8$ K after 3×10^7 yr, or to 10^{10} K in a Hubble time.[7] Therefore, the NTB emission phase must be very short-lived. A possible way to circumvent the rapid cooling of the hotter plasma by conduction or rapid energy loss of the nonthermal particles is to physically separate these from the cooler ICM gas. Exactly how this can be done is difficult to determine, but strong magnetic fields or turbulence may be able to produce such a situation.

In what follows we assume the IC process as the working hypothesis for the origin of the HXR flux. However, in view of the above-mentioned difficulties more observations are acutely needed to determine the HXR emission process. Such observations are challenging: thermal emission from clusters of galaxies can be well characterized as thermal bremsstrahlung with emission lines due to atomic transitions, with a characteristic temperature of a about a few to ∼15 keV. This means that any reliable detection of the nonthermal component relies on an instrument sensitive above at least 10 keV. Sensitive measurements require instruments employing focusing optics, but no such instruments are currently operational. We must therefore rely on the collimated detectors on board *BeppoSAX* or *RXTE* or the *Suzaku* Hard X-ray Detector (HXD), but for such instruments, good limiting sensitivity requires long observations. Therefore, the target selection, based on a good prediction of the HXR flux, requires careful consideration of all aspects of the phenomenon.

The most important selection criterion is the presence of diffuse radio emission. About 40 clusters are known to have such emission, which can be classified as halo or relic (see Giovannini et al. 1999; Giovannini & Feretti 2000; Feretti et al. 2000). The fraction of clusters with diffuse radio emission rises with SXR luminosity (Giovannini et al. 1999), which is in turn correlated with temperature, via $L_{\rm SXR} \propto T^2$ (see, e.g., Allen & Fabian 1998), indicating a correlation of the nonthermal activity with temperature. In addition, turbulence and shocks, present in merging

[6] These expressions are valid for $p > 3$ or $\Gamma > 2$. For smaller indices an upper energy limit $\gamma_{\rm max}$ also must be specified and the above expressions must be modified by other factors that are omitted here for the sake of simplification.

[7] These estimates are based on energy losses of electrons in a cold plasma, which is an excellent approximation for electron energies $E \gg kT$. As E nears kT the rate of loss of energy decreases and the bremsstrahlung yield increases. For $E/kT > 4$ this increase will be at most about a factor of 2.

TABLE 1
OBSERVED AND ESTIMATED PROPERTIES OF CLUSTERS

Cluster (1)	z (2)	kT[a] (keV) (3)	$F_{1.4\ \mathrm{GHz}}$[b] (mJy) (4)	θ[b,c] (arcmin) (5)	F_{SXR}[d] (F_0) (6)	B[e] (μG) (7)	F_{HXR}[d,f] (F_0) (8)
Coma	0.023	7.9	540	30	33	0.70	4.7 (1.6)
A2256	0.058	7.5	400	12	5.1	1.1	1.8 (1.0)
1ES 0657−558	0.296	15.6	78	5	3.9	1.2	0.52 (0.5)
A2219	0.226	12.4	81	8	2.4	0.86	1.0
MACS J0717	0.550	13	220	3	3.5	2.6	0.76
A2163	0.208	13.8	55	6	3.3	0.97	0.51
A2744	0.308	11.0	38	5	0.76	1.0	0.41
A1914	0.171	10.7	50	4	1.8	1.3	0.22

[a] From Allen & Fabian (1998), except 1ES 0657−558 data from Liang et al. (2000).
[b] From Giovannini et al. (1999) and Giovannin & Feretti 2000, except 1ES 0657−558 data from Liang et al. (2000).
[c] Approximate largest angular extent.
[d] $F_0 = 10^{-11}$ ergs cm^{-2} s^{-1}.
[e] Estimates based on equipartition.
[f] Estimates assuming $\zeta\gamma_{\min} = 10^6$, with observed values in parentheses for Coma from Rephaeli et al. (1999), Rephaeli & Gruber (2002), and Fusco-Femiano et al. (1999, 2004) and for A2256 by Fusco-Femiano et al. (2000, 2005) and Rephaeli & Gruber (2003).

clusters, are the most likely agents of acceleration and could be the cause of the higher temperatures, as well as the nonthermal activity. Consequently, high temperatures and the presence of substructure also must influence the selection (see Buote 2001; Schuecker et al. 2001). Note that higher temperatures make the detection of the HXR flux more difficult. However, at higher redshifts this effect is offset by the spectral redshift $z \equiv Z - 1$. Based on the criteria given above, a list of some of the most promising clusters is given in Table 1.

These are only qualitative criteria, but for the IC model one can give some quantitative estimates. At a redshift $z \equiv Z - 1$ the CMB energy $u \propto Z^4$ and the critical frequency $\nu_{c,\mathrm{IC}} \propto Z$. As a result the ratio of IC to synchrotron fluxes

$$\mathcal{R} = F_{\mathrm{HXR}}/F_{\mathrm{radio}} \propto Z^{2+\Gamma}/B_{\perp}^{\Gamma}, \tag{2}$$

so for an observed radio flux one would like to choose clusters with the lowest magnetic field B and the highest redshifts. Unfortunately, the B field strengths in most of the diffuse radio-emitting clusters are not known (Coma is an exception), so one must rely on some theoretical arguments to estimate the value of B. If we assume some proportional relation (e.g., equipartition) between the energies of the magnetic field and nonthermal electrons,

$$\mathcal{E}_e = N_{\mathrm{total}}\frac{p-1}{p-2}\gamma_{\min}mc^2 = \zeta\frac{B^2}{8\pi}\frac{4\pi R^3}{3}, \tag{3}$$

where $R = \theta d_A/2$ is the radius of the (assumed) spherical cluster with the measured angular diameter θ and angular diameter distance $d_A(Z)$, and equipartition with electrons is equivalent to $\zeta = 1$.

From equations (1)–(3) we can determine the three unknowns B, $\mathcal{E}_e$ (or N_{total}), and F_{HXR} purely in terms of ζ, $\gamma_{\min}$, and the observed quantities (given in Table 1) z, θ, and the radio flux

$$\nu F_{\mathrm{radio}}(\nu) = cr_0^2 N_{\mathrm{total}} A_{\mathrm{synch}}(p)(p-1)\gamma_{\min}^{p-1}\left(\frac{B^2}{8\pi}\right) \times \left(\frac{Z\nu}{\nu_{\mathrm{cr,\,synch}}}\right)^{2-\Gamma}\left[4\pi d_L^2(Z)\right]^{-1}, \tag{4}$$

where $d_L = d_A Z^2 = (c/H_0)Zr(Z)$ is the luminosity distance to a source with the comoving coordinate $r(Z)$. The result is[8]

$$\left(\frac{B}{\mu\mathrm{G}}\right)^{\Gamma+2} = 0.20\zeta^{-1}\left[\frac{F(1.4\ \mathrm{GHz})}{\mathrm{Jy}}\right]\left(\frac{5'}{\theta}\right)^3\left(\frac{10^4}{\gamma_{\min}}\right)^{2\Gamma-3}\frac{Z^{3-\Gamma}}{r(Z)}, \tag{5}$$

$$N_{\mathrm{total}} = 2.3\times10^{65}\frac{\Gamma-3/2}{\Gamma-1}\zeta\left(\frac{10^3}{\gamma_{\min}}\right)\left(\frac{\theta}{5'}\right)^3\left(\frac{B}{\mu\mathrm{G}}\right)^2\left[\frac{r(Z)}{Z}\right]^3, \tag{6}$$

$$\epsilon F_{\mathrm{HXR}}(\epsilon) = 0.034F_0\left(\frac{N_{\mathrm{total}}}{10^{65}}\right)\left(\frac{10^4}{\gamma_{\min}}\right)^{2\Gamma-4} \times \left(\frac{\epsilon}{5.9\ \mathrm{keV}}\right)^{2-\Gamma}\left[\frac{Z}{r(Z)}\right]^2, \tag{7}$$

where we have defined $F_0 \equiv 10^{-11}$ ergs cm^{-2} s^{-1}. Note also that in all these expressions one can use the substitution $R = (3.39\ \mathrm{Mpc})(\theta/5')r(Z)/Z$.

To obtain numerical estimates of the above quantities, in addition to the observables F_{radio}, θ, and redshift z we need the values of ζ and $\gamma_{\min}$. Very little is known about these two parameters and how they may vary from cluster to cluster. From the radio observations at the lowest frequency we can set an upper limit on $\gamma_{\min}$; for Coma, e.g., $\gamma_{\min} < 4\times10^3(\mu\mathrm{G}/B)$. We also know that the cutoff energy cannot be too low because that would require an excessive amount of energy (for $p > 3$) that would go into heating of the ICM gas via Coulomb collisions. A conservative estimate would be $\gamma_{\min} \sim 10^3$. Even less is known about ζ. The estimated values of the magnetic fields B for the simple case of $\Gamma = 2$, equipartition (i.e., $\zeta = 1$), and low-energy cutoff $\gamma_{\min} = 10^3$ are given in the column (7) of Table 1. As expected these are of the order of a few microgauss; for significantly stronger field,

[8] Here we have set the Hubble constant $H_0 = 70$ km s^{-1} Mpc^{-1}, the CMB temperature $T_0 = 2.8$ K, and the radio frequency $\nu = 1.4$ GHz. In general $B^{2+\Gamma} \propto H_0\nu^{\Gamma-1}$, $N_{\mathrm{total}} \propto H_0^{-3}$, and $F_{\mathrm{HXR}} \propto H_0^2 T_0^{2+\Gamma}$. We have also assumed an isotropic distribution of the electron pitch angles and set $B = B_{\perp}(4/\pi)$.

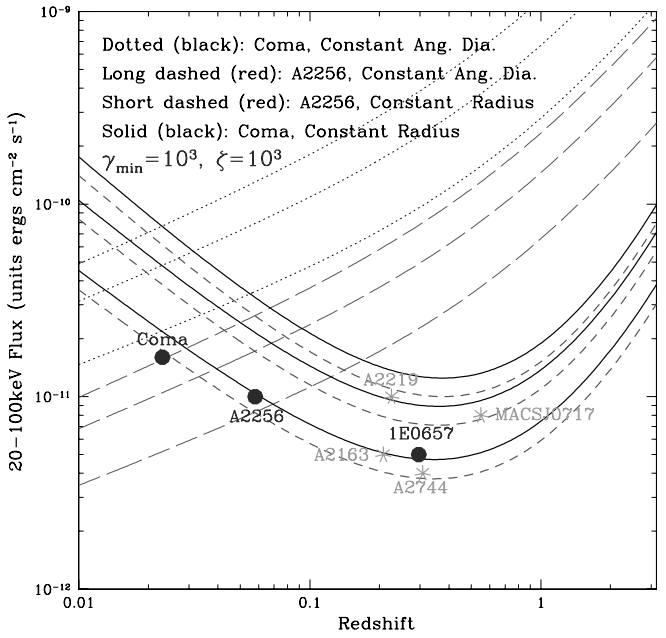


FIG. 1.—Predicted variations of the HXR flux with redshift assuming a constant metric (*solid and short-dashed lines*) or angular diameters (*dotted and long-dashed lines*), using the Coma Cluster (*black lines*) and A2256 (*gray lines*) parameters assuming $\zeta = \gamma_{min} = 10^3$. In each group the IC photon spectral index $\Gamma = 2.25$, 2.0, and 1.75 (*from top to bottom*). Filled circles are based on observations, and asterisks are based on the estimates given in Table 1. [*See the electronic edition of the Journal for a color version of this figure.*]

the predicted HXR fluxes would be below what is detected (or even potentially detectable). For $\Gamma = 2$ the magnetic field $B \propto (\zeta\gamma_{min})^{-1/4}$ and $F_{HXR} \propto (\zeta\gamma_{min})^{1/2}$, so for sub-microgauss fields and $F_{HXR} \sim F_0$ we need $\zeta\gamma_{min} \sim 10^6$. Assuming $\gamma_{min} = 10^3$ and $\zeta = 10^3$ we have calculated the expected fluxes integrated in the range of 20–100 keV (which for $\Gamma = 2$ is equal to $1.62[(20\ \mathrm{keV})F_{HXR}(20\ \mathrm{keV})]$) shown in column (8) of Table 1. The variation of this flux with redshift based on the observed parameters, θ and $F_{radio}(\nu = 1.4\ \mathrm{GHz})$, of Coma and A2256 is plotted in Figure 1 for $\Gamma = 1.75$, 2.0, and 2.25 ($p = 2.5$, 3 and 3.5) and assuming a constant metric radius R, which is a reasonable assumption. We also plot the same assuming a constant angular diameter. This could be the case due to observational selection bias if most diffuse emission is near the resolution of the telescopes. These are clearly uncertain procedures and can give only semiquantitative measures. However, the facts that the Coma and A2256 have the highest fluxes and that our observations of 1ES 0657−558, described below, yield a flux close to our predicted value is encouraging. Clearly, all the other clusters in Table 1 are similarly promising candidates for future HXR observations.

3. OBSERVATIONS AND ANALYSIS

3.1. *Description of Observations*

Cluster 1ES 0657−558 was observed with *RXTE* during 95 separate pointings from 2002 August 19 to 2003 April 3, collecting approximately 400,000 s of data. After filtering the Proportional Counter Array (PCA) data by following the standard selection criteria, we obtained a total of 309,630 s of good PCA data. During the campaign, only Proportional Counter Unit (PCU) 0 and PCU 2 were on. Since PCU 0 had lost its propane guard layer, in order to ensure that we have the best possible calibration, we used only the PCU 2 detector. The selection criteria involved excluding data obtained when the detector pointing was more than $0.^{\circ}02$ off the source, excluding data obtained when the Earth elevation angle was less than 10°, and excluding times near passage through the South Atlantic Anomaly (SAA), which caused large variations in the count rate.

The amount of good time for each of the two High-Energy X-Ray Timing Experiment (HEXTE) detector clusters is about one-third that for the PCA data: 105,450 s for cluster A and 105,510 s for cluster B. The ratio of HEXTE net time to PCA net time is reasonable, since each HEXTE cluster spent half of the time for background measurement and a fraction of the time was lost due to electronic dead time caused by cosmic rays.

The PCA background was estimated using the FTOOL `pcabackest` (ver. 3.0) with the "L7/240" model provided by the *RXTE* GOF (Guest Observer Facility). The estimator program used the model known as `pcabkgdcmfaint17eMv20051128.mdl` as the background model, which in turn took into consideration the instantaneous particle-induced intrinsic instrument background and activation, mainly due the SAA passages, as well as the cosmic X-ray background. We note here that the above background model, available from HEASARC at NASA Goddard Space Flight Center (C. Markwardt 2006, private communication), allows robust estimate of background up to ~30 keV even for faint sources such as 1ES 0657−558.

We used the top layer of PCU 2 in the 3–30 keV range. The mean background-subtracted PCU 2 count rate was 1.418 ± 0.007 counts s^{-1} in the top layer over this band. For the response matrix, we used the standard PCA response matrix, generated via the `pcarsp` software tool (ver. 10.1), as appropriate to the beginning of the observations (2002 August); while the *RXTE* PCA response matrix changes with time, the change is gradual, and the values of spectral fits obtained using the matrix appropriate for the end of the observations (2003 April) showed no discernible difference. For HEXTE, the background-subtracted count rates over the 20–70 keV energy band were 0.0103 ± 0.0227 and 0.0700 ± 0.0192 counts s^{-1} for HEXTE detector clusters A and B, respectively; above 70 keV, the source was not clearly detected. We used the standard redistribution files, `xh97mar20c_pwa_64b.rmf` and `xh97mar20c_pwb013_64b.rmf`, with the standard HEXTE effective area files available through HEASARC.

While *RXTE* clearly detected the cluster, inclusion of higher spectral resolution data allows a better constraint on the temperature of the thermal component and thus better constraints on the nature of the nonthermal emission. To this end, we considered the published *Advanced Satellite for Cosmology and Astrophysics* (*ASCA*) data, but because the best statistical accuracy was provided in the *XMM-Newton* data, we extracted and analyzed archival spectra collected during the *XMM-Newton* pointing in 2000 October 20–21. We reduced the data using a procedure described in Andersson & Madejski (2004), but here we used the XMMSAS20050815 release of the *XMM-Newton* data analysis software. We screened the data against any obvious flares; this meant any segments of data with a total count rate greater than 12 counts s^{-1} for pn and 4.5 counts s^{-1} for either MOS. After cleaning, the effective exposure times are 24,916 s for the MOS1 data, 24813 s for the MOS2 data, and 21,704 s for the pn data. We note that a detailed analysis of the *XMM-Newton* data for this cluster, in particular the analysis of the spatial structure, will be presented in K. Andersson et al. (2006, in preparation). For all three *XMM-Newton* detectors, we extracted source counts from a region of $4'$ radius around the centroid of the count distribution. For the background, we used an annulus with inner and outer radii of $8'$ and $12'$, with all obvious point sources removed. We also removed the data corresponding to the Cu K line in the pn camera, corresponding to 7.9–8.2 keV spectral range. The data

were grouped to include at least 40 counts bin^{-1} for the pn data files and 25 counts bin^{-1} for the MOS data files. We used the standard instrument resolution matrices and effective area files as released in the SAS version as above. In the subsequent analysis, we restricted the two MOS and pn data sets to the 1–10 keV range, to avoid any residual cross calibration problems between the three instruments.

3.2. *Analysis and Spectral Fitting*

3.2.1. *RXTE Data*

We first present an analysis of the *RXTE* observations and then present a joint analysis of the *RXTE* and *XMM-Newton* data. In all subsequent fits we fix the redshift at 0.296. The models consist of a MEKAL thermal emission component, in which we also allow a second component, either thermal or a power law. We first use a single thermal MEKAL model to fit the *RXTE* data. The model includes cold absorption due to neutral gas in the line of sight in our Galaxy. Since the *RXTE* data alone do not constrain the Galactic column density, we fix this parameter at 4.6×10^{20} cm^{-2}, the value from radio measurements but also consistent with the best fit to *ASCA* data (Liang et al. 2000). We note that all errors quoted correspond to 90% confidence limits.

The best-fit temperature under an assumption of a simple, one-temperature MEKAL model is 12.1 ± 0.4 keV. This is in moderate agreement with the value $14.5^{+2.0}_{-1.7}$ keV determined from a joint fit to the *ROSAT* and *ASCA* data (Liang et al. 2000) and the value $14.8^{+1.7}_{-1.2}$ keV from the *Chandra X-Ray Observatory* (Markevitch et al. 2002). The metal abundance is $A = 0.16 \pm 0.04$ solar, which is moderately lower than the value $A = 0.33 \pm 0.16$ from the joint *ROSAT* and *ASCA* data but is in good agreement with the *Chandra* value of 0.11 ± 0.11. The best-fit model yields χ^2 of 114 for 98 degrees of freedom (dof). The ratio of the *RXTE* data to the best-fit MEKAL model indicates a systematic upward rise above 10 keV, suggesting that an extra component may be required. If we adopt this secondary component to be a power law, then χ^2 is 102 (96 dof), with poorly determined index ($\Gamma > 2$). The 90% confidence interval of the power-law flux in the 20–100 keV range is $(0.3 \pm 0.2)F_0$. We thus conclude that even from the *RXTE* data alone, we have a marginal but suggestive detection of hard X-ray flux in 1ES 0657−558.

3.2.2. *XMM-Newton Data*

The *XMM-Newton* data extracted as above were first fitted to a model including absorption due to neutral gas with solar abundances and a thermal (MEKAL) plasma. Since the absolute calibration of the three *XMM-Newton* detectors might vary, we allowed the respective normalizations not to be tied to one another. The best-fit absorption was close to the value inferred from the radio data of Liang et al. (2000), with the column $(2.8 \pm 1.0) \times 10^{20}$ cm^{-2}, but here inclusion of the MOS data below 1 keV altered the resulting best-fit column to $(5 \pm 0.5) \times 10^{20}$ cm^{-2}. We concluded that the column derived from the *XMM-Newton* data is consistent with 4.6×10^{20} cm^{-2} cited by Liang et al. (2000) and used that value in all subsequent fits. The temperature of the MEKAL component was 12.0 ± 0.5 keV and elemental abundances 0.24 ± 0.04 solar, consistent with all data sets above. The fit is acceptable, at $\chi^2 = 1367$ for 1408 dof.

3.2.3. *Joint RXTE and XMM-Newton Data*

In the analysis below, we include both the *RXTE* and *XMM-Newton* data, since the very good effective area of the instrument coupled with good spectral resolution of its detectors allows tighter constraints on spectral parameters for the emission detected below ~10 keV and thus mainly on the thermal component. However, the only reliable approach here is to perform the spectral fitting simultaneously.

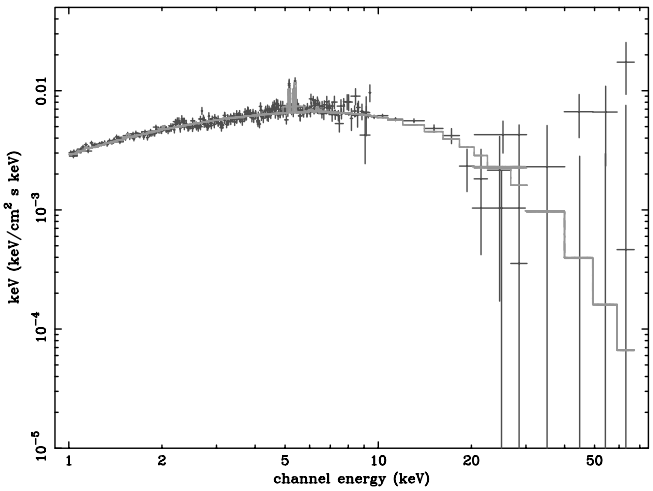


FIG. 2.—Unfolded spectrum of the cluster 1ES 0657−558, where the *XMM-Newton* and *RXTE* data were fitted with a single-temperature thermal (MEKAL) model, plotted here as the solid histogram. For clarity, prior to plotting, the *XMM-Newton* data were scaled by a cross normalization factor, close to unity, to agree with the *RXTE* data. [*See the electronic edition of the Journal for a color version of this figure*.]

The joint analysis of the *RXTE* and *XMM-Newton* data provides more evidence of the need for a secondary component. We use the *XMM-Newton* and *RXTE* data over the bandpasses as above; we allow the normalization of the *RXTE* instruments to be different from that for the *XMM-Newton* instruments, which in turn are allowed to vary among themselves. A single isothermal (MEKAL) fit yields an adequate fit, with χ^2 of 1483 for 1508 dof. The hydrogen column density n_{H} is $(2.8 \pm 1.0) \times 10^{20}$ cm^{-2}, which is marginally lower than the Galactic value of Liang et al. (2000; see the discussion above); in the subsequent fits we adopt the value of Liang et al. (2000) of 4.6×10^{20} cm^{-2}. Regardless of the exact value of the absorption, the plasma temperature is 12.1 ± 0.2 keV and elemental abundances are 0.19 ± 0.03 solar. We note that the true errors on those quantities are only approximate, since as pointed out by Markevitch et al. (2002, 2004), this cluster shows some temperature structure, while we use an average temperature.

Adding a power-law component to the isothermal model improves the χ^2 value, which is now 1464 for 1506 dof. Such change in χ^2 with addition of two parameters is very significant (at more than 99.9%). The temperature in this case decreases to 11.2 ± 0.8 keV. The photon index is 1.6 ± 0.3 and the nonthermal flux in the 20–100 keV energy band is $(0.5 \pm 0.2)F_0$. In the context of statistical significance of raw counting rates, at energies above 20 keV, where the power-law model dominates, the excess (over the value predicted by the thermal model) corresponds to ~0.8 and 2.8 σ for HEXTE cluster A and B, respectively. For the purpose of illustration, we show the unfolded spectrum of the data fitted to a single-temperature thermal model in Figure 2, while Figure 3 shows the confidence levels of two fit parameters, photon index versus the flux of the nonthermal component, for our preferred two-component model.

Alternatively, this secondary, hot component can be modeled via another thermal plasma spectral component. Using this parameterization (and assuming that only the temperature and normalization differ from the lower T-component), we inferred its

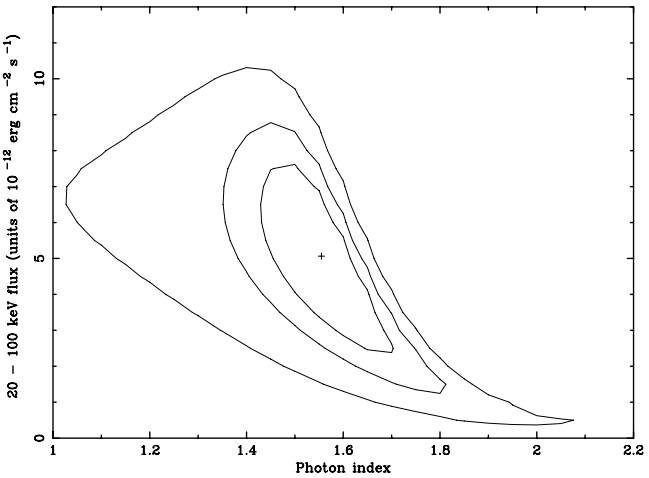


FIG. 3.—Confidence regions (corresponding to $\chi^2_{\rm min} + 2.3$, 4.6, and 9.2) on the best-fit parameters for the spectral fits to the joint *XMM-Newton*, *RXTE* PCA, and HEXTE data for cluster 1ES 0657−558 for the photon index of the nonthermal X-ray component and its 20–100 keV flux (in units of 10^{-12} ergs cm^{-2} s^{-1}). See the text for details.

temperature to be 50 (>30) keV. The 20–100 keV flux of this component is also $(0.5 \pm 0.2)F_0$. Now the lower T-component has a temperature of 10.1 ± 0.9 keV. While we cannot definitely exclude this interpretation on the grounds of the quality of fit (χ^2 is 1471 for 1506 dof), we argue in § 4 that the power-law spectral shape provides for a more viable interpretation of the secondary component.

4. SUMMARY AND DISCUSSION

Radio observations of diffuse emission from ICM show the presence of nonthermal activity in many clusters, especially in those with high SXR emitting gas temperatures (and luminosity) and showing recent merger activity. A list of such clusters is shown in Table 1. Detections of HXR emission exceeding the levels expected from the thermal gas have been reported by two groups using different instruments. This enables a quantitative investigation of the nature and origin of the nonthermal activity. The radio observations alone indicate the presence of extremely relativistic electrons ($\gamma \sim 10^4$). Assuming equipartition between the relativistic electrons and the magnetic field we estimate a volume-averaged magnetic field value in the range of 0.5–2 μG (see Table 1), in rough agreement with (line-of-sight averaged) field strengths deduced from Faraday rotation measurements. In the case of Coma the magnetic field deduced from Faraday rotation of 2–3 μG implies conditions far from equipartition if we assume a homogeneous source; the field energy density is about 25 times larger than that of the electrons. This discrepancy can be resolved by an inhomogeneous model, e.g., the two-phase model proposed by Brunetti et al. (2001) that implies a magnetic field profile, or if there is 25 times more energy in nonthermal protons than in electrons.

If the HXR radiation is due to IC scattering of CMB photons by the same electrons that produce the synchrotron radio emission, which we have argued to be the simplest scenario, such high magnetic fields would imply IC fluxes in the 20–100 keV range of about $10^{-2}F_0$, while both Coma and A2256 show fluxes higher than F_0. Production of HXRs at this level requires magnetic fields of about 0.1 μG (or a partition parameter $\zeta \sim 10^3$), which raises the required energy density of the nonthermal electrons ($\mathcal{E}_e \propto \zeta^{1/2}$). For example, for Coma and A2256 the observed

TABLE 2

PARAMETERS FROM SPECTRAL FITTINGS

PARAMETER	VALUE		
	Single Thermal	Double Thermal	Thermal + Power Law
	RXTE		
$n_{\rm H}/10^{20}$ cm^{-2}	4.6[a]	...	4.6[a]
kT_1 (keV)	12.1 ± 0.4	...	11.7 ± 0.5
kT_2 (keV)	...	...	...
Abundance[b]	0.16 ± 0.04	...	0.25 ± 0.08
Photon index	...	...	>2
$F^{100\ {\rm keV}}_{20\ {\rm keV}}/F_0$[c]	...	...	0.3 ± 0.2
χ^2/dof	114/98	...	102/96
	RXTE and *XMM-Newton*		
$n_{\rm H}/10^{20}$ cm^{-2}	2.8 ± 1.0	4.6[a]	4.6[a]
kT_1 (keV)	12.1 ± 0.2	10.1 ± 0.9	11.2 ± 0.8
kT_2 (keV)	...	50 (>30)	...
Abundance[b]	0.19 ± 0.03	0.19 ± 0.03	0.22 ± 0.04
Photon index	...	...	1.6 ± 0.2
$F^{100\ {\rm keV}}_{20\ {\rm keV}}/F_0$[c]	...	0.5 ± 0.3	0.5 ± 0.3
χ^2/dof	1483/1508	1471/1506	1464/1506

[a] Parameter fixed at the given value.
[b] Solar.
[c] $F_0 = 10^{-11}$ ergs cm^{-2} s^{-1}.

HXR fluxes require $\mathcal{E}_e = 2 \times 10^{-13}$ and 1.5×10^{-12} ergs cm^{-3}, respectively, which are comparable to the energy density of the CMB (4.6×10^{-13} ergs cm^{-3}). By assuming similar conditions for other clusters, several years ago we identified 1ES 0657−558 and A2219 as possible candidates for having detectable HXR fluxes. Here we have described these observations of 1ES 0657−558 and the results of our spectral fitting to these data alone and to the *RXTE* data combined with the SXR data from *XMM-Newton*. In the future, attempts should be made to observe the other clusters listed in Table 1 and any newly discovered cluster with a relatively high temperature and redshift, an ample sign of substructure and/or mergers, and, of course, strong diffuse radio emission. A low value of magnetic field indicated by Faraday rotation measurements or estimated via equipartition argument would also be good justification for HXR observations.

We have shown that a thermal component plus a nonthermal tail described as a power law with spectral index $\Gamma = 1.6$ containing $\sim 0.5F_0$ of the 20–100 keV flux provides an acceptable fit. This flux is fortuitously close to the value of $0.52F_0$ we estimate by scaling the Coma and A2256 observations. (Note that the equipartition [i.e., $\zeta = 1$] magnetic field and flux for this cluster would be ~ 1 μG and $0.02F_0$, respectively.) This agreement is somewhat encouraging, so we believe that the chances are even better for detection of HXR emission from Abell 2219, a good candidate at a moderate redshift, and a recently discovered cluster, MACS J0717, with even higher z than 1ES 0657−558. As is the case for Coma and A2256, these clusters also require high nonthermal electron energy densities: $\mathcal{E}_e = [1.0, 1.8, 8.5] \times 10^{-13}$ ergs cm^{-3} for A2219, 1ES 0657−558, and MACS J0717, respectively. These are even closer to the CMB densities at their respectively higher redshifts. In general the required electron energies are about 1%–10% of the energy density of the thermal gas of few $\times 10^{-11}$ ergs cm^{-3}, which is also comparable to the gravitational potential energy density of the cluster. This means a very efficient acceleration process.

Regarding the spectral fits to 1ES 0657−558, as shown in Table 2, we also obtain an acceptable fit with a double-temperature thermal model with a second component with $kT = 50$ keV and a normalization implying a volume emission measure (EM) for this component that is a significant fraction ($\sim$10%) of that of the lower temperature component. Indeed, Markevitch (2005) finds evidence for such a high T-component behind the shock near the Bullet Cluster based on recent *Chandra* data. However, this has a much smaller EM than is required for fitting the data with a two-temperature model. In fact a high T-component with such a large EM would have been easily detected by Markevitch (2005). Clearly more and deeper observations of the clusters in Table 1 could clarify this situation considerably. In particular, deep observations with imaging HXR instruments, such as the proposed *Nuclear Spectroscopic Telescope Array* (*NuSTAR*) satellite, that could provide information about the spatial distribution of the HXRs would be very valuable.

In spite of the uncertainties on the exact character of the observed radiation spectra and the emission mechanism and in spite of the meagerness of the data, the acceleration mechanism of electrons can be constrained significantly. The lifetimes of electrons with energies in the range 200 keV $\leq E \leq$ 200 GeV are longer than the crossing time, $T_{\rm cross} \sim 3 \times 10^6$ yr. Therefore, these electrons will escape the cluster and radiate most of their energy outside the cluster unless there exists some scattering agent with a mean free path $\lambda_{\rm scat} \sim 1$ kpc to trap the electrons in the ICM for at least a timescale of $T_{\rm esc} = (R/\lambda_{\rm scat})T_{\rm cross} \sim 3 \times 10^9$ yr, for cluster size $R \sim 1$ Mpc. Turbulence could be this agent and could play a role directly in stochastic acceleration or indirectly in acceleration by shocks, presumably arising from merger events. Several lines of argument point to an ICM that is highly turbulent, and there has been considerable discussion of these aspects of the problem in the recent literature (see, e.g., Cassano & Brunetti 2005). These aspects are explored in P01, but the upshot is that *we require injection of high-energy electrons, presumably from galaxies and active galactic nuclei (AGNs), and that the acceleration process is episodic on a timescale of* $\sim 10^8$–10^9 *yr.* Whether the electrons are injected directly by past and current AGN activity or are produced by the interaction with the thermal gas of cosmic-ray protons escaping the galaxies would be difficult to determine now. There are, however, constraints on both these scenarios (see, e.g., Blasi 2003).

This work was supported by NASA ADP grant NNG04GA66G-NCX, by *Chandra* grants GO1-2113X and GO4-5125X from NASA via the Smithsonian Astrophysical Observatory, and by Department of Energy contract to SLAC DE-AC3-76SF00515. We acknowledge help in reducing the *XMM-Newton* data by Karl Andersson, and we thank Craig Markwardt for providing us with the updated *RXTE* PCA background information.

REFERENCES

Allen, S. A., & Fabian, A. C. 1998, MNRAS, 297, L57
Andersson, K., & Madejski, G. 2004, ApJ, 607, 190
Blasi, P. 2000, ApJ, 532, L9
———. 2003, in ASP Conf. Ser. 301, Matter and Energy in Clusters of Galaxies, ed. S. Bowyer & C.-Y. Hwang (San Francisco: ASP), 203
Bowyer, S. 2003, in ASP Conf. Ser. 301, Matter and Energy in Clusters of Galaxies, ed. S. Bowyer & C.-Y. Hwang (San Francisco: ASP), 125
Brunetti, G., Setti, G., Feretti, L., & Giovannini, G. 2001, MNRAS, 320, 365
Buote, D. A. 2001, ApJ, 553, L15
Carilli, C., & Taylor, G. B. 2002, ARA&A, 40, 319
Cassano, R., & Brunetti, G. 2005, MNRAS, 357, 1313
Clarke, T. E. 2003, in ASP Conf. Ser. 301, Matter and Energy in Clusters of Galaxies, ed. S. Bowyer & C.-Y. Hwang (San Francisco: ASP), 185
Clarke, T. E., Kronberg, P. P., & Böhringer, H. 2001, ApJ, 547, L111
Enßlin, T. A., Lieu, R., & Biermann, P. 1999, A&A, 344, 409
Feretti, L., Brunetti, G., Giovannini, G., Govoni, F., & Setti, G. 2000, in Constructing the Universe with Clusters of Galaxies, ed. F. Durret & D. Gerbal (Paris: CNRS), 37
Feretti, L., Fusco-Femiano, R., Giovannini, G., & Govoni, F. 2001, A&A, 373, 106
Fusco-Femiano, R., dal Fiume, D., Feretti, L., Giovannini, G., Grandi, P., Matt, G., Molendi, S., & Santangelo, A. 1999, ApJ, 513, L21
Fusco-Femiano, R., Landi, R., & Orlandini, M. 2005, ApJ, 624, L69
Fusco-Femiano, R., Orlandini, M., Brunetti, G., Feretti, L., Giovannini, G., Grandi, P., & Setti, G. 2004, ApJ, 602, L73
Fusco-Femiano, R., Orlandini, M., De Grandi, S., Molendi, S., Feretti, L., Giovannini, G., Bacchi, M., & Govoni, F. 2003, A&A, 398, 441
Fusco-Femiano, R., et al. 2000, ApJ, 534, L7
Giovannini, G., & Feretti, L. 2000, NewA, 5, 335
Giovannini, G., Feretti, L., Venturi, T., Kim, K.-T., & Kronberg, P. 1993, ApJ, 406, 399
Giovannini, G., Tordi, M., & Feretti, L. 1999, NewA, 4, 141
Govoni, F., & Feretti, L. 2004, Int. J. Mod. Phys. D, 13, 1549
Govoni, F., Feretti, L., Murgia, M., Taylor, G., Giovannini, G., & Dallacasa, D. 2003, in ASP Conf. Ser. 301, Matter and Energy in Clusters of Galaxies, ed. S. Bowyer & C.-Y. Hwang (San Francisco: ASP), 501
Gruber, D., & Rephaeli, Y. 2002, ApJ, 565, 877
Hudson, D. S., Henriksen, M. J., & Colafrancesco, S. 2003, ApJ, 583, 706
Kim, K.-T., Kronberg, P. P., Dewdney, P. E., & Landecker, T. L. 1990, ApJ, 355, 29
Liang, H., Hunstead, R. W., Birkinshaw, M., & Andreani, P. 2000, ApJ, 544, 686
Lieu, R., Mittaz, J. P. D., Bowyer, S., Breen, J. O., Lockman, F. J., Murphy, E. M., & Hwang, C.-Y. 1996, Science, 274, 1335
Markevitch, M. 2005, in The X-Ray Universe 2005, ed. A Wilson (ESA SP-604; Noordwijk: ESA), 723
Markevitch, M., Gonzalez, A. H., Clowe, D., Vikhlinin, A., Forman, W., Jones, C., Murray, S., & Tucker, W. 2004, ApJ, 606, 819
Markevitch, M., Gonzalez, A. H., David, L., Vikhlinin, A., Murray, S., Forman, W., Jones, C., & Tucker, W. 2002, ApJ, 567, L27
Petrosian, V. 1973, ApJ, 186, 291
———. 2001, ApJ, 557, 560 (P01)
Rephaeli, Y. 1979, ApJ, 227, 364
Rephaeli, Y., & Gruber, D. 2002, ApJ, 579, 587
———. 2003, ApJ, 595, 137
Rephaeli, Y., Gruber, D., & Arieli, Y. 2006, ApJ, 649, 673
Rephaeli, Y., Gruber, D., & Blanco, P. 1999, ApJ, 511, L21
Rossetti, M., & Molendi, S. 2004, A&A, 414, L41
Rudnick, L., & Blundell, K. M. 2003, ApJ, 588, 143
Rybicki, G., & Lightman, A. 1979, Radiative Processes in Astrophysics (New York: Wiley)
Schlickeiser, R., Sievers, A., & Thiemann, H. 1987, A&A, 182, 21
Schuecker, P., Böhringer, H., Reiprich, T. H., & Feretti, L. 2001, A&A, 378, 408
Thierbach, M., Klein, U., & Wielebinski, R. 2003, A&A, 397, 53